J Electroceram
DOI 10.1007/s10832-014-9901-9

A comparative study of high temperature properties of cobalt-free perovskites

J. F. Basbus · F. D. Prado · A. Caneiro · L. V. Mogni

Received: 14 October 2013 / Accepted: 4 February 2014

Abstract Co-free perovskites with chemical composition $Ba_{0.5}Sr_{0.5}Fe_{0.8}M_{0.2}O_{3-\delta}$ (M = Ni, Cu, Zn) were synthesized by the modified Pechini method, and their structure and microstructure were characterized by XRD and SEM. Oxygen content, electrical resistivity and Thermal Expansion Coefficient (TEC) were evaluated in air between room temperature and 900 °C. The high-temperature properties of these perovskites were compared with those of Co containing $Ba_{0.5}Sr_{0.5}Fe_{0.8}Co_{0.2}O_{3-\delta}$ perovskite. The highest electrical conductivity was obtained for $Ba_{0.5}Sr_{0.5}Fe_{0.8}Cu_{0.2}O_{3-\delta}$, with values of 47.6 Scm^{-1} at 544 °C. This same composition also exhibits the highest oxygen vacancies concentration: 3-δ = 2.61 at room temperature. In contrast, the $Ba_{0.5}Sr_{0.5}Fe_{0.8}Zn_{0.2}O_{3-\delta}$, showed lower electrical conductivity suggesting that the Zn^{+2} ions block electron transport. Co-free perovskites seem to be stable at high temperatures for long term periods. However, these compounds suffered degradation at room temperature in samples stored in air.

Keywords Cobalt-free perovskite · SOFC cathode · Oxygen separation membranes · $Ba_{0.5}Sr_{0.5}Fe_{0.8}M_{0.2}O_{3-\delta}$ · Dilatometry · Conductivity

J. F. Basbus
Centro Atómico Bariloche, CNEA-AGNPCyT, Av Bustillo 9500, CP 8400 S.C de Bariloche, Argentina
e-mail: basbus@cab.cnea.gov.ar

F. D. Prado
CONICET, Universidad Nacional de Sur, Alem 1253, CP 8000 Bahía Blanca, Argentina
e-mail: fernando.prado@uns.edu.ar

A. Caneiro · L. V. Mogni (✉)
Centro Atómico Bariloche, CNEA-CONICET, Av Bustillo 9500, CP 8400 S.C de Bariloche, Argentina
e-mail: mogni@cab.cnea.gov.ar

A. Caneiro
e-mail: caneiro@cab.cnea.gov.ar

1 Introduction

Cobalt-rich perovskites such as $Sm_{0.5}Sr_{0.5}CoO_{3-\delta}$ [1], $La_xSr_{1-x}Fe_yCo_{1-y}O_3$ [2–5] $LnBaCo_2O_{5+\delta}$ [6–10], $Ba_{0.5}Sr_{0.5}Co_{0.8}Fe_{0.2}O_{3-\delta}$ [11], have been extensively studied as cathode materials for intermediate temperature solid oxide fuel cells (IT-SOFC) or oxygen separation membranes due to their high catalytic activity for the reduction of molecular oxygen. This property is related to high electronic conductivity and the presence of oxygen vacancies, which promote ionic conductivity. However, these mixed conductors present drawbacks such as high values of thermal expansion coefficients (TEC) compared to more common electrolytes, poor chemical stability in CO_2, easier evaporation and reduction of Co, and high cost. Furthermore, instability of the cubic phase below 1000 °C has also been reported in cobalt-rich barium perovskites, with the formation of a mixture of cubic and 12H hexagonal phases in $Ba_xSr_{1-x}Co_{0.8}Fe_{0.2}O_{3-\delta}$, with x > 0.2 [12]. These features limit the applicability of Co-rich oxides and prompt the search for cobalt-free perovskite cathodes.

Cobalt-free perovskites with chemical composition $Ba_{0.5}Sr_{0.5}Zn_{0.2}Fe_{0.8}O_{3-\delta}$ [13–15], $Ba_{0.5}Sr_{0.5}Cu_{0.2}Fe_{0.8}O_{3-\delta}$ [16, 17], $Sm_{0.5}Sr_{0.5}Fe_{0.8}Cu_{0.2}O_{3-\delta}$ [18] have showed interesting results as cathodes for IT-SOFC and oxygen separation membranes. However, to the best of our knowledge, no comparative and systematic studies have evaluated the effect of transition metals (Ni, Cu, Zn) on the high temperature properties of the $Ba_{0.5}Sr_{0.5}Fe_{0.8}M_{0.2}O_{3-\delta}$ perovskites. With this aim, we have synthesized cubic $Ba_{0.5}Sr_{0.5}Fe_{0.8}M_{0.2}O_{3-\delta}$ (M = Ni, Cu, Zn) perovskites in order to examine the effect of temperature variation on properties such as electrical conductivity, thermal expansion, oxygen content and lattice parameter. Particularly, the $Ba_{0.5}Sr_{0.5}Fe_{0.8}Ni_{0.2}O_{3-\delta}$ is a novel composition reported for the first time in the present work. The $Ba_{0.5}Sr_{0.5}Fe_{0.8}Co_{0.2}O_{3-\delta}$ oxide is also characterized in

Published online: 18 February 2014

order to compare its high-temperature properties with those of Co-free perovskites.

2 Experimental

2.1 Sample preparation and characterization

The $Ba_{0.5}Sr_{0.5}Fe_{0.8}M_{0.2}O_{3-\delta}$ (M = Co, Ni, Cu and Zn) powders were synthesized by the modified Pechini method [14] with citric acid and EDTA as chelating agent. Previously, metallic nitrates were obtained dissolving $BaCO_3$, $SrCO_3$, Fe, Co, Ni, Cu and Zn (>99.99 %) with nitric acid. The obtained resins were burnt at 400 °C during 6 h with subsequent heat treatments in order to obtain the perovskite phases. The optimum synthesis temperature was found testing between 600 and 1250 °C for $Ba_{0.5}Sr_{0.5}Fe_{0.8}Ni_{0.2}O_{3-\delta}$.

The crystal structure and the phase purity were examined by X-ray diffraction (XRD) using a Philips PW1700 diffractometer with CuKα radiation and a graphite monochromator. The crystal structure and the amount of secondary phases were analyzed by the Rietveld method using FullProf suite tools [19]. All samples showed cubic symmetry with space group *Pm-3m*. The microstructural characterization of the obtained powders was performed by scanning electron microscopy (SEM) using a SEM-FEG FEI NOVA-Nano 230 microscope.

Dense samples for electrical conductivity and dilatometry measurements were obtained by uniaxially pressing the $Ba_{0.5}Sr_{0.5}Fe_{0.8}M_{0.2}O_{3-\delta}$ powders at 100 kg/cm^2 and sintering at high temperatures. Table 1 shows the labels used to identify each sample, the temperatures of the powder synthesis and those temperatures used for pellet sintering.

2.2 High-temperature properties

The structural stability of the cubic phase and lattice parameter variation as functions of temperature were analyzed in-situ by XRD at high temperature (HT-XRD). This study was performed between room temperature and 900 °C under stationary air using an Anton Paar camera coupled with the Philips PW1700 diffractometer. The lattice parameters were determined by means of sequential mode using FullProf suite tools.

Oxygen content (3-δ) as a function of temperature in synthetic air was determined by thermogravimetry using a symmetrical thermobalance based on a Cahn 1000 electrobalance [20]. With the exception of BSFZn, the absolute oxygen content of the samples was determined by reduction in dry 20 % H_2/Ar at 1000 °C, considering BaO, SrO, Fe° and M° (M° = Co°, Ni°, Cu°) as final products. Due to the high vapor pressure of metallic Zn, the 3-δ oxygen content for the BSFZn sample was determined by partial reduction under inert gas at 950 °C. The formation of $Ba_{0.5}Sr_{0.5}Fe_{0.8}Zn_{0.2}O_{2.4}$ was assumed complete when the mass remained constant at 950 °C. The perovskite structure of this composition, where all Fe is Fe^{3+} ($Ba_{0.5}Sr_{0.5}Fe_{0.8}Zn_{0.2}O_{2.4}$), was confirmed by XRD.

The lattice expansion of these samples was determined from dilatometry in air atmosphere between room temperature and 900 °C under a heating-cooling rate of 1 °C/min, using a vertical LINSEIS L75VS1000C Dilatometer.

The electrical conductivity measurements were performed by the four-probe method using an Agilent 3497A scanner-multimeter. The evolution of conductivity with temperature was studied in air between room temperature and 900 °C under a heating/cooling rate of 1 °C/min.

The phase stability of samples was checked by XRD after heat treatment at 600 and 700 °C during more than 200 h.

2.3 Study of room temperature degradation

A non-linear behavior of the lattice parameter between room temperature and 400 °C was detected in samples stored in air at room temperature. In these samples, the lattice parameter increased with temperature up to 400 °C, then decreased. This behavior was only observed in the first heating cycle. This fact and the observation by SEM of segregated products at grain boundaries in all the $Ba_{0.5}Sr_{0.5}Fe_{0.8}M_{0.2}O_{3-\delta}$ perovskites, indicates a possible degradation of samples. One of the compositions, the BSFCu sample, was chosen in order to further investigate the possible mechanisms behind such degradation. The surface of samples stored for a period of 30 days was observed by SEM, and compared with a refreshed sample obtained after a heat treatment at 800 °C. Mass evolution as a temperature function for the long-term stored BSFCu sample was followed by thermogravimetry between room temperature and 500 °C through two heating and cooling consecutive cycles. The thermal behavior for the same sample was analyzed by Differential Scanning Calorimetry (DSC) with a Modulated DSC 2910 TA Instruments at a heating rate of 5 °C/min between room temperature and 500 °C in air. Two consecutive cycles were also performed.

Table 1 Listed synthesis and sintering temperatures of each sample. Lattice parameter *a* obtained from XRD data is also included

Composition	Label	T synthesis (°C)	T sintering (°C)	*a* (Å)
$Ba_{0.5}Sr_{0.5}Fe_{0.8}Co_{0.2}O_{3-\delta}$	BSFCo	950	1150	3.9560
$Ba_{0.5}Sr_{0.5}Fe_{0.8}Ni_{0.2}O_{3-\delta}$	BSFNi	1250	1250	3.9531
$Ba_{0.5}Sr_{0.5}Fe_{0.8}Cu_{0.2}O_{3-\delta}$	BSFCu	800	1000	3.9353
$Ba_{0.5}Sr_{0.5}Fe_{0.8}Zn_{0.2}O_{3-\delta}$	BSFZn	950	1250	3.9883

3 Results and discussion

3.1 Sample characterization

The substitution of Co by another transition metal in the $Ba_{0.5}Sr_{0.5}Fe_{0.8}M_{0.2}O_{3-\delta}$ perovskite must fulfill the Goldschmidt tolerance factor [21]:

$$t = \frac{r_A + r_O}{\sqrt{2}(r_B + r_O)}$$

where r_A, r_B, and r_O are the radii of the A-site cation, B-site cation, and oxide ion, respectively. The cubic structure is considered to be stable within the range $0.9 \leq t \leq 1.0$. For $Ba_{0.5}Sr_{0.5}Fe_{0.8}Co_{0.2}O_{3-\delta}$, t is estimated to be between 0.998 and 1.041, slightly larger than the optimum value. Similar t values were calculated for Cu and Zn substituted samples, while the substitution of Co by Ni increases the t factor to over 1.40, due to the small radii of Ni. Therefore, it is expected that the $Ba_{0.5}Sr_{0.5}Fe_{0.8}Ni_{0.2}O_{3-\delta}$ compound would present a hexagonal structure instead of a cubic one.

Figure 1a shows the XRD data of BSFNi powder obtained at different temperatures. A secondary NiO phase is observed for all temperatures, with a minimum of 2.2 %wt of NiO at 1250 °C. Despite the high t-factor, the resulting perovskite $Ba_{0.5}Sr_{0.5}Fe_{0.8}Ni_{0.2}O_{3-\delta}$ presents cubic symmetry with the *Pm-3m* space group determined by Le Bail method [22] using Fullprof suite tools [19]. This result is analogous to that reported by Ding et al. for the $Ba_{0.5}Sr_{0.5}Fe_{0.9}Ni_{0.1}O_{3-\delta}$ composition [23]. The XRD data for this novel composition was refined by the Rietveld method assuming cubic symmetry. Figure 1b shows the observed and calculated intensities, the differences between these and the (hkl) Bragg position resulting in a lattice parameter a=3.9531(2) Å and goodness factors χ^2=7.36, R_{wp}=18.3, R_{exp}=7.30 and R_p=19.8.

The XRD data from BSFCo, BSFNi, BSFCu and BSFZn samples are shown in Fig. 2. The lattice parameters obtained from the Rietveld refinement are listed in Table 1. The BSFCu, BSFNi and BSFZn samples exhibit a minoritary 2.5 % CuO, 2.2 % NiO and 2.7 % ZnO phases, respectively. The peaks of these secondary phases are shown in the insert of Fig. 2.

The a-lattice parameter at room temperature shows a systematic decrease with the atomic number of the M ion, with the exception of the Zn-substituted sample. The lattice parameter found for BSFZn is similar to that previously reported [13–15]. In this case, the increase of the lattice parameter for BSFZn is likely due to the higher ionic radius of 0.74 Å for Zn^{+2}, while the samples with Co, Ni and Cu ions show mixed valences and reach higher valence states, therefore lowering ionic radii, such as 0.54 Å for Cu^{+3} instead of 0.73 Å for Cu^{+2}.

The microstructures of $Ba_{0.5}Sr_{0.5}Fe_{0.8}M_{0.2}O_{3-\delta}$ powders are shown in Fig. 3. The BSFCo and BSFZn, obtained at 950 °C, present well connected micrometric grains. These microstructures are quite different from that of BSFCu, where the lower temperature of synthesis produces poorly connected agglomerates constituted by submicrometric grains. The BSFNi obtained at 1250 °C, presents a different microstructure constituted by particles of about 100 nm forming large agglomerates. The presence of isolated NiO particles is also detected in agreement with that observed by XRD. Therefore, the BSFCu shows an optimum microstructure for applications such as SOFC cathodes, where large surface areas play a fundamental role in improving electrode performance.

3.2 High-temperature properties

Phase stability and oxygen content (3-δ) as a function of temperature were investigated in air between room temperature and 900 °C, combining HT-XRD and thermogravimetry techniques. This study was performed in order to evaluate the

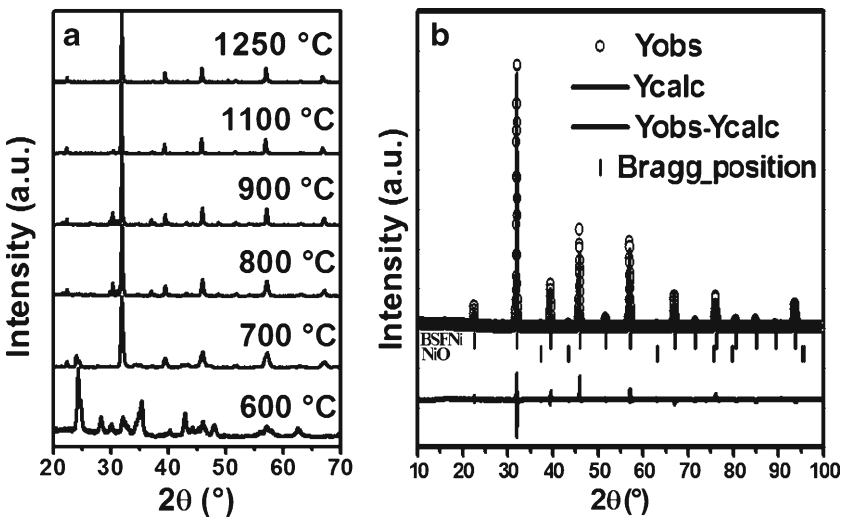

Fig. 1 (**a**) Evolution of XRD pattern as a function of synthesis temperature for BSFNi. (**b**) Rietveld refinement result for BSFNi obtained at 1250 °C

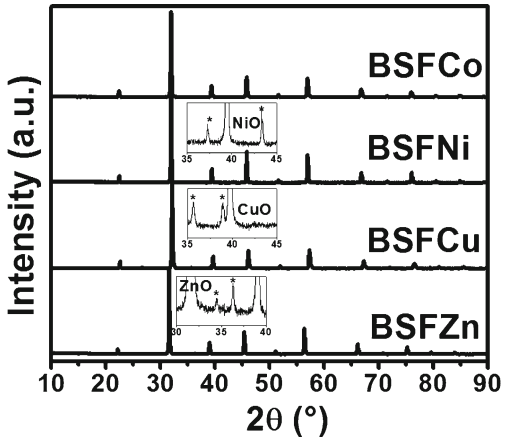

Fig. 2 XRD patterns of as obtained $Ba_{0.5}Sr_{0.5}Fe_{0.8}M_{0.2}O_{3-\delta}$ samples. The inserts show the peaks corresponding to the secondary phases

effect of oxygen content on crystal structure. Figure 4 shows the evolution of 3-δ and the lattice parameter vs. temperature for BSFCo, BSFNi, BSFCu and BSFZn samples. All samples exhibit cubic symmetry across the entire range of temperatures. The lattice parameters increase moderately until they reach the temperature corresponding to the start of oxygen loss, after which the rate of change increases faster. Similar values of lattice parameters and oxygen content have been reported by other authors for samples with the same composition. The oxygen content decreases as the atomic number of the cations increases following the trend: Co>Ni>Cu≅Zn. This relationship is consistent with the decreasing trend for the stabilization of higher oxidation states in the series Co, Ni, Cu, Zn. While Co and Ni could present +2, +3 or even +4 oxidation states, Cu could exhibit +2 and +3, and Zn only +2. Furthermore, despite of the fact that for both BSFZn and BSFCu compounds the oxygen content between room temperature and 900 °C takes almost the same values, the change of lattice parameter in the same range of temperature is higher for the BSFCu sample. This difference could be associated with the presence of Cu^{+3} ions at room temperature, which are reduced to Cu^{+2} as T increases. According to the oxygen content at room temperature for the BSFZn sample, Zn^{+2} (r_{Zn+2}=0.74 Å) should coexist with $Fe^{+2/+3}$ (r_{Fe+2}=0.78 Å and r_{Fe+3}=0.645 Å, considering both as High Spin). However, $Cu^{+2/+3}$ (r_{Cu+2}=0.73 Å and r_{Cu+3}=0.54 Å) could be present besides $Fe^{+2/+3}$ ions in the BSFCu sample. Therefore, the partial substitution of Fe^{+3} by Cu^{+3} should be responsible for the lower lattice parameter of the BSFCu sample compared to that of BSFZn at room temperature.

Figure 5 shows the linear expansion ($\Delta L/L_0$) as a function of T, where ΔL is the change of length and L_0 the initial length at 20 °C. These measurements were carried out using heating-cooling rates of 1 °C/min in air. Changes in slopes are observed at temperatures where oxygen losses from the structures start. Table 2 shows the thermal expansion coefficients, $\text{TECs} = \frac{\Delta L / L_0}{\Delta T}$, obtained from dilatometry and HT-XRD in air. These values were obtained from the temperature range before and after the observed break in curves for each sample and for the whole temperature range, 20≤T≤900 °C. There are differences between the TECs values obtained through lattice parameters and dilatometry for all compositions, except for the BSFCo. Nevertheless, these values are higher than

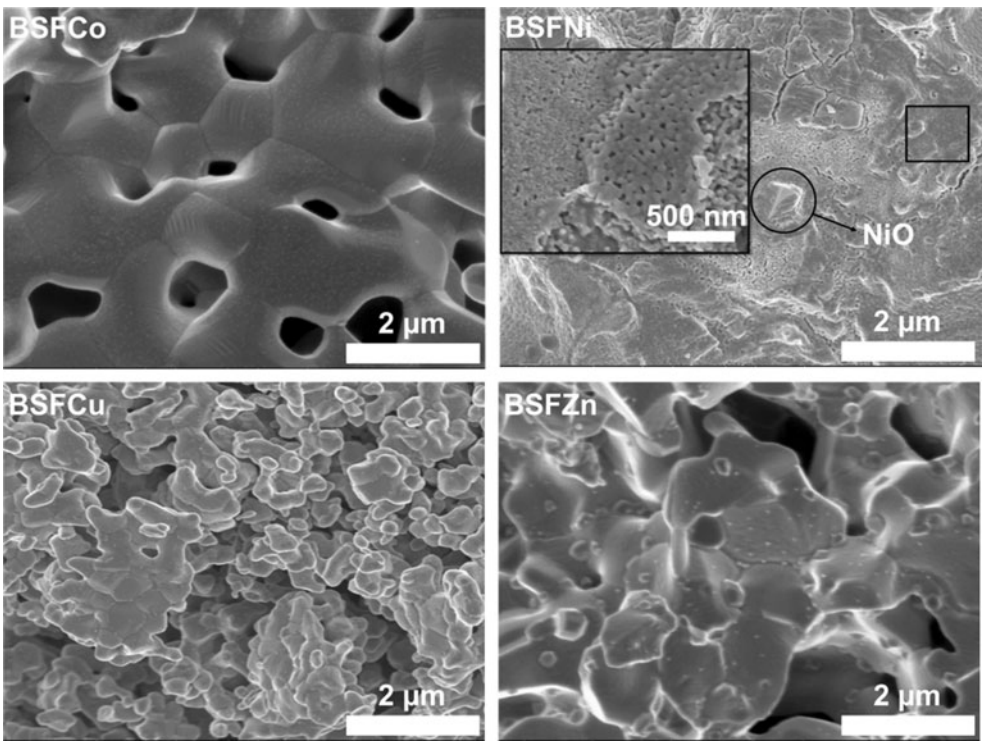

Fig. 3 SEM pictures of $Ba_{0.5}Sr_{0.5}Fe_{0.8}M_{0.2}O_{3-\delta}$ powders obtained at different temperatures

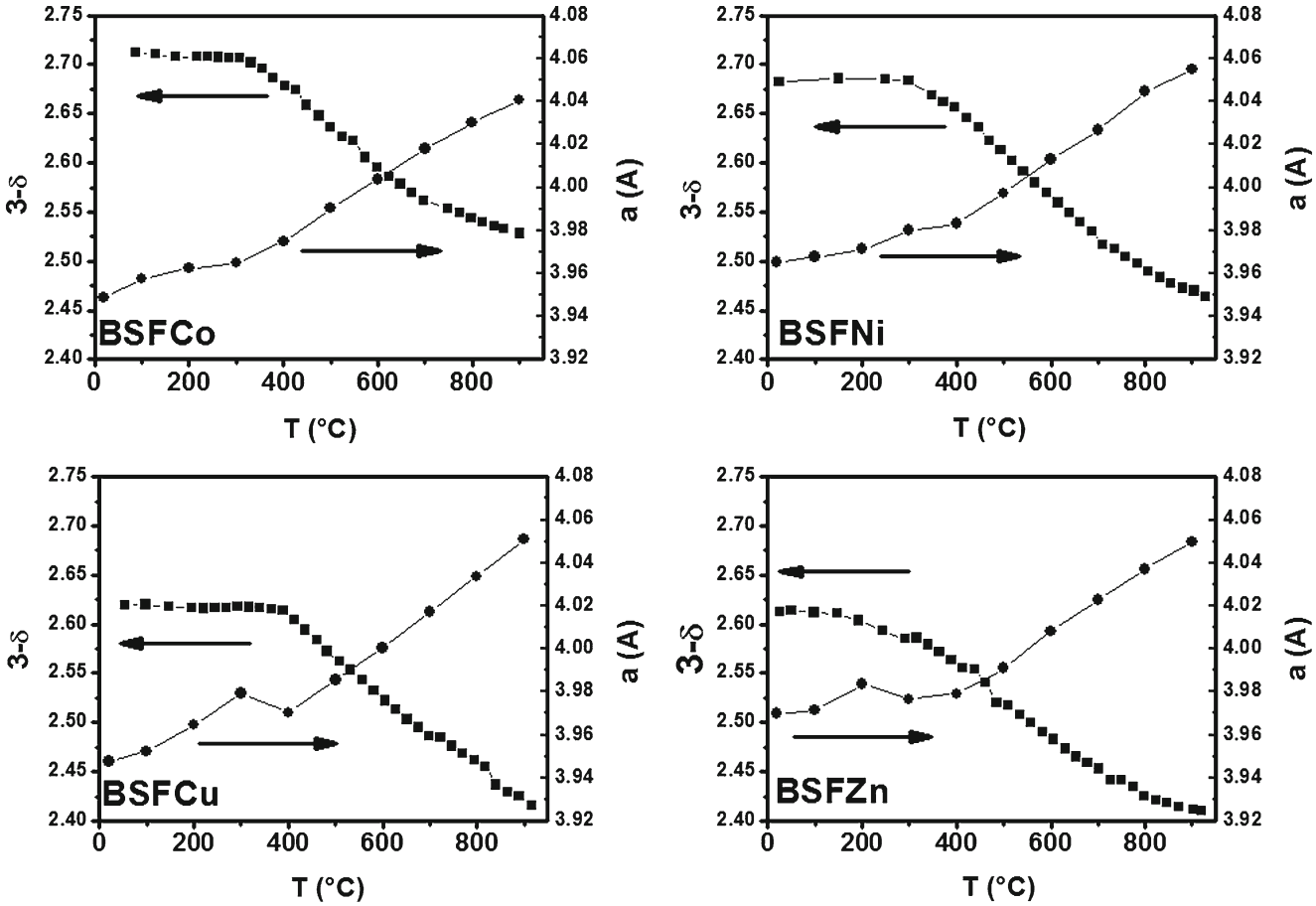

Fig. 4 Equilibrium oxygen content (3-δ) and lattice parameter (*a*) as a function of T in air for $Ba_{0.5}Sr_{0.5}Fe_{0.8}M_{0.2}O_{3-\delta}$ (M = Co, Ni, Cu, Zn)

those previously reported by other authors. For example, Zhu et al. [24] presented TEC=23 10^{-6} K^{-1} between 25 and 850 °C for $Ba_{0.5}Sr_{0.5}Fe_{0.8}Co_{0.2}O_{3-\delta}$, which is lower than that found in the current study (27.1 10^{-6} K^{-1}). Higher differences exist

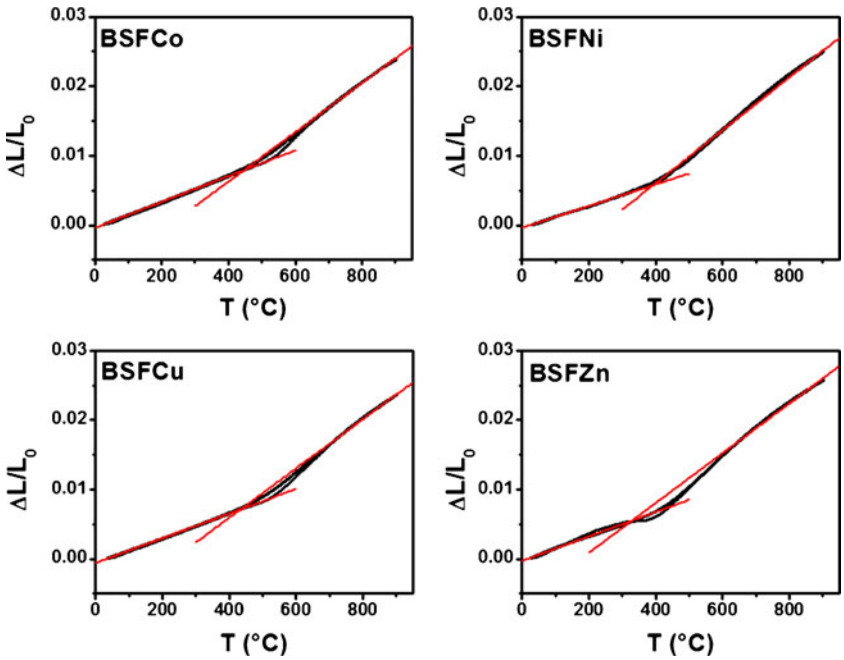

Fig. 5 Linear expansion ($\Delta L/L_0$) as a function of T in air for $Ba_{0.5}Sr_{0.5}Fe_{0.8}M_{0.2}O_{3-\delta}$

Table 2 Thermal expansion coefficients TECsobtained from dilatometry $\left(\frac{\Delta L/L_0}{\Delta T}\right)$ and from HT-XRD $\left(\frac{\Delta \alpha/\alpha_0}{\Delta T}\right)$ in air. The TECs for the high and low temperature region are also included

Sample	TEC ($10^{-6}K^{-1}$)					
	Dilatometry			HT-XRD		
	20–350 °C	600–900 °C	20–900 °C	20–300 °C	600–900 °C	20–900 °C
BSFCo	18.3	36.7	27.1	15.4	30.6	26.5
BSFNi	16.6	36.3	28.5	13.7	35.0	25.8
BSFCu	17.4	38.8	27.2	14.5	41.7	29.7
BSFZn	16.5	35.3	29.1	19.2	34.4	22.8

between our TEC values for BSFCu and BSFZn samples and those reported in literature [25–27]. While for $Ba_{0.5}Sr_{0.5}Fe_{0.8}Cu_{0.2}O_{3-\delta}$ Efimov et al. [25] and Park et al. [26] found TECs between 20.5 10^{-6} K^{-1} and 25.8 10^{-6} K^{-1} by HT-XRD and dilatometry, respectively, Luo et al. reported for $Ba_{0.5}Sr_{0.5}Fe_{0.8}Zn_{0.2}O_{3-\delta}$ a TEC=10.5 10^{-6} K^{-1} between 300 and 1400 °C [27]. These differences could arise from the experimental procedure. In our case, the HT-XRD measurements were performed after equilibrating time and dilatometry were recorded under a low heating rate (1 °C/min). These conditions, closer to thermodynamic equilibrium, allow the evolution of the oxygen content, giving values lower than those of samples forced to follow higher heating rates. Therefore, under equilibrium, a major effect of the chemical expansion associated with changes in the oxygen content is expected. Finally, it could be observed that the TEC values of these cobalt-free perovskites are even higher than those of the most common electrolytes.

Conductivity data as a function of temperature is shown in Fig. 6. All samples exhibit the same semiconductor-type behavior: conductivity increases with T until the temperature where oxygen loss begins, after which conductivity is similar to that of metals. Similar to what happens in other perovskites, this metallic-type conductivity is due to a decrease in the charge carrier concentration as the oxygen content decreases, suggesting a p-type conductivity with electron–hole charge carriers. Table 3 summarizes the maximum conductivity reached and the activation energies of our samples. The higher activation energy, together with a fixed Zn^{+2} valence, justify the lower values of electrical conductivity for the BSFZn sample. These conductivities values are also in agreement with those previously reported by other authors [15]. These authors found that by increasing the Zn content for the $Ba_{0.5}Sr_{0.5}Co_{0.2-x}Zn_xFe_{0.8}O_{3-\delta}$ compounds, conductivity decreases due to the fact that zinc blocks the electrical conduction because it maintains a static bivalent state.

Otherwise, the BSFCu and BSFNi samples show lower activation energies, which, together with the tendency of both compounds to present mixed and lower valences than Co ions, induce Fe to exist in $Fe^{+3/+4}$ state and to increase the electron–hole concentration. The electrical conductivity of the BSFCu

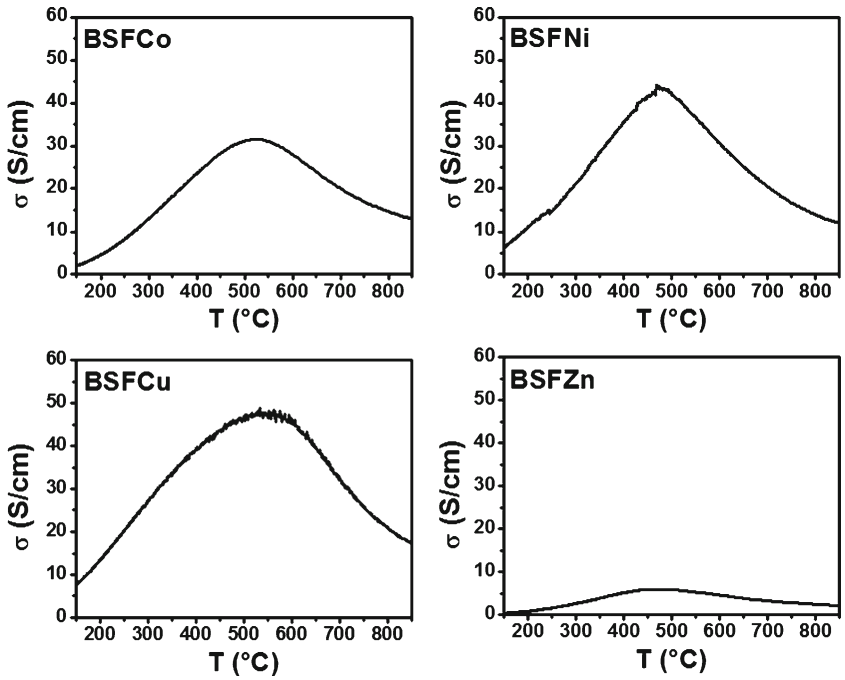

Fig. 6 Electrical conductivity (σ) as a function of T in air for $Ba_{0.5}Sr_{0.5}Fe_{0.8}M_{0.2}O_{3-\delta}$

Table 3 Maximum electrical conductivity values with corresponding temperatures and activation energy (E_a) in the low temperature range for each sample

Sample	*T max (°C)*	*σ max* (Scm^{-1})	E_a (*eV*)
BSFCo	522	31.5	0.292
BSFNi	478	43.3	0.214
BSFCu	544	47.6	0.205
BSFZn	474	6.0	0.326

sample is similar to those previously reported by other authors [16, 17, 28], which along with that of BSFNi, is higher than those of cobalt rich perovskites such as $Ba_{0.5}Sr_{0.5}Co_{0.8}Fe_{0.2}O_{3-\delta}$ [29].

Finally, in these Co-free perovskites the cubic phase is stable when it undergoes a long-term treatment at temperature below 700 °C, contrary to what was observed for Co-rich barium perovskites in previous studies [12]. No change in XRD pattern was observed after heat treatment at 600 and 700 °C during more than 200 h.

3.3 Room temperature degradation

A slow degradation mechanism acts on the samples when they are stored in air at room temperature. This degradation can be observed by SEM of a BSFCu sample stored for more than 30 days (Fig. 7). A surface segregated phase is observed at the grain boundaries. Neither the change in composition nor the change in structure have been detected in the segregated phases by either EDS or XRD, respectively. The segregated layer disappears after a heat treatment at 800ºC, as is shown in Fig. 3c. To analyze the origin of this degradation, two consecutive thermogravimetric cycles were performed between room temperature and 500 °C (see Fig. 8a). Three mass losses at 100, 250 and 400 °C, could be distinguished in the first cycle increasing T. The second completed cycle perfectly superimposes with the first decreasing T cycle. It is well-known that barium perovskites undergo degradation at high temperature

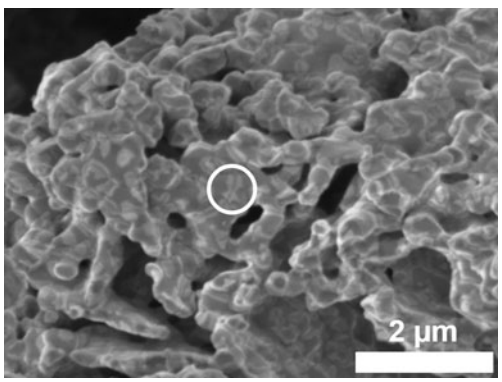

Fig. 7 SEM of BSFCu sample stored in air during 30 days. The *white circle* marks the segregated compounds in the grain boundary zone

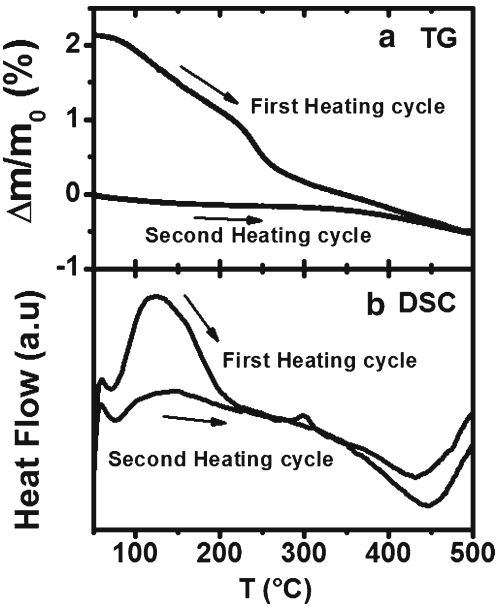

Fig. 8 (**a**) Thermogravimetric and (**b**) Differential Scanning Calorimetry cycling between 20 and 500 °C of BSFCu sample stored for 30 days at room temperature in air

in atmospheres containing CO_2 and H_2O [30]. However, no degradation at room temperature has been reported. In our case, the irreversible mass loss around 100 and 240 °C could be ascribed to desorption of H_2O and CO_2 from the surface [30], while the reversible loss at 400 °C was attributed to the oxygen loss. Figure 8b shows a DSC study where, in the first heating cycle, two endothermic peaks associated with desorption processes are observed at 100 and 250 °C. These peaks disappear in the second cycle (see Fig. 8b). These results are in agreement with the TG measurements. Therefore, the slow degradation of samples stored in air at room temperature could be due to the adsorption of H_2O and CO_2 on the sample surface near grain boundary zones. This degradation did not affect the structure of samples and was reversible under cycling between room temperature and 800 °C.

4 Conclusions

The comparative study of lattice parameters and oxygen content as a function of temperature for the cubic $Ba_{0.5}Sr_{0.5}Fe_{0.8}M_{0.2}O_{3-\delta}$ (M = Co, Ni, Cu and Zn) perovskites opens discussion of the oxidation states of the transition metals in these materials and explains the thermal expansion and conductivity results.

Comparing the changes in lattice parameter and oxygen content with temperature leads to the conclusion that while the Zn is present as an invariant Zn^{+2} state, the Co, Ni and even the Cu, exhibit mixed valence states. Additionally, the oxygen content values decrease as the atomic number increases following the series Co > Ni > Cu ≅ Zn according the facility of

each compound to stabilize at high oxidation states. While Co and Ni could be present as +2, +3 and even +4 state, the higher valences that could exhibit Cu and Zn ions are +3 and +2, respectively.

In contrast with the results previously reported [25–27], the TEC values of these cobalt-free perovskites are higher than those of most common electrolytes, making these materials unsuitable for SOFC application from a thermo-mechanical point of view.

All compositions exhibit a semiconductor behavior, increasing σ with T until reaching the oxygen removal temperature, where the conductivity changes to a metallic-type. In these samples, the conductivities are even higher than those of cobalt-rich perovskites such as $Ba_{0.5}Sr_{0.5}Co_{0.8}Fe_{0.2}O_{3-\delta}$. The relative conductivity values suggest that for BSFCu and BSFNi samples, the capability of Cu and Ni to present mixed and lower valence than Co ions induces Fe cations to exist as $Fe^{+3/+4}$. Therefore, the electron–hole concentration and the p-type conductivity rise for BSFCu and BSFNi compared with BSFCo samples. Otherwise, in the BSFZn composition, the fixed Zn^{+2} valence reduces the conductivity abruptly because of the static bivalent state, which blocks the conduction path.

Finally, a slow degradation was observed in samples stored in air at room temperature. This reversible degradation could be ascribed to the adsorption of H_2O and CO_2 on sample surface nearer to grain boundary zones. The samples can be restored after a treatment at high temperatures.

Acknowledgments This work was supported by CNEA (Argentine Atomic Energy Commission), CONICET (Argentine Research Council), UNCuyo and ANPCyT. The authors thank Prof. N. Gonzalez and Mr. Alex Ferrari for English revision of this manuscript.

References

1. L. Yang, C. Zuo, S. Wang, Z. Cheng, M. Liu, Adv. Mater. **20**, 3280 (2008)
2. E.P. Murray, M. Sever, S. Barnett, Solid State Ionics **148**, 27 (2002)
3. N. Grunbaum, L. Dessemond, J. Fouletier, F. Prado, L. Mogni, A. Caneiro, Solid State Ionics **180**, 1448 (2009)
4. N. Grunbaum, L. Dessemond, J. Fouletier, F. Prado, A. Caneiro, Solid State Ionics **177**, 907 (2006)
5. L. Baqué, A. Caneiro, M.S. Moreno, A. Serquis, Electrochem. Commun. **10**, 1905 (2008)
6. J.-H. Kim, L. Mogni, F. Prado, A. Caneiro, J.A. Alonso, A. Manthiram, J. Electrochem. Soc. **156**, B1376 (2009)
7. N. Li, Z. Lü, B. Wei, X. Huang, K. Chen, Y. Zhang, W. Su, J. Alloys Compd. **454**, 274 (2008)
8. J.-H. Kim, F. Prado, A. Manthiram, J. Electrochem. Soc. **155**, B1023 (2008)
9. J.H. Kim, A. Manthiram, J. Electrochem. Soc. **155**, B385 (2008)
10. A. Tarancón, A. Morata, G. Dezanneau, S.J. Skinner, J.A. Kilner, S. Estradé, F. Hernández-Ramírez, F. Peiró, J.R. Morante, J. Power Sources **174**, 255 (2007)
11. Z. Shao, S.M. Haile, Nature **431**, 170 (2004)
12. C. Niedrig, S. Taufall, M. Burriel, W. Menesklou, S.F. Wagner, S. Baumann, E. Ivers-Tiffée, Solid State Ionics **197**, 25 (2011)
13. B. Wei, Z. Lü, X. Huang, M. Liu, N. Li, W. Su, J. Power Sources **176**, 1 (2008)
14. B. Wei, Z. Lü, X. Huang, Z. Liu, J. Miao, N. Li, W. Su, J. Am. Ceram. Soc. **90**, 3364 (2007)
15. J. Park, J. Zou, H. Yoon, G. Kim, J.S. Chung, Int. J. Hydrogen Energy **36**, 6184 (2011)
16. L. Zhao, B. He, Y. Ling, Z. Xun, R. Peng, G. Meng, X. Liu, Int. J. Hydrogen Energy **35**, 3769 (2010)
17. L. Zhao, B. He, X. Zhang, R. Peng, G. Meng, X. Liu, J. Power Sources **195**, 1859 (2010)
18. Y. Ling, J. Yu, B. Lin, X. Zhang, L. Zhao, X. Liu, J. Power Sources **196**, 2631 (2011)
19. J. Rodriguez-Carvajal. Abstr. Satell. Meet. Powder Diffr. XV Congr. IUCr, Toulouse, Fr. **127**, (1990)
20. A. Caneiro, P. Bavdaz, J. Fouletier, J.P. Abriata, Rev. Sci. Instrum. **53**, 1072 (1982)
21. V. Goldschmidt, Naturwissenschaften **14**, 477 (1926)
22. A. Le Bail, Powder Diffract. **20**, 316 (2012)
23. Y. Ding, Y. Chen, X. Lu, B. Lin, Int. J. Hydrogen Energy **37**, 9830 (2012)
24. Q. Zhu, T. Jin, Y. Wang, Solid State Ionics **177**, 1199 (2006)
25. K. Efimov, T. Halfer, A. Kuhn, P. Heitjans, J.J. Caro, A. Feldhoff, Chem. Mater. **22**, 1540 (2010)
26. C.Y. Park, T.H. Lee, S.E. Dorris, J.-H. Park, U. Balachandran, J. Power Sources **214**, 337 (2012)
27. H.X. Luo, L.H. Yu, X.Z. Chen, H.H. Wang, J. Caro, Chin. Chem. Lett. **20**, 250 (2009)
28. S. Shahgaldi, Z. Yaakob, D.J. Khadem, M. Ahmadrezaei, W.R.W. Daud, J. Alloys Compd. **509**, 9005 (2011)
29. B. Wei, Z. Lü, X. Huang, J. Miao, X. Sha, X. Xin, W. Su, J. Eur. Ceram. Soc. **26**, 2827 (2006)
30. E. Bucher, A. Egger, G.B. Caraman, W. Sitte, J. Electrochem. Soc. **155**, B1218 (2008)